

UNIVERSIDAD DE CÓRDOBA

Facultad de Ciencias

Grado de Física

Trabajo Fin de Grado

Luminescent response study of ionic crystals
used in dosimetry

Código del TFG: **FS24-008-FSC**

Tipo de TFG: **Trabajo de iniciación a la investigación**

Autor: Marta de la Rosa Núñez



Acknowledgments

Incluir los agradecimientos, si procede.

Contents

General index	2
Index of Figures	5
Index of tables	6
Resumen. Palabras clave	7
Abstract. Keywords	8
1 Introduction	9
2 Objectives	11
3 Theoretical framework	13
3.1 The mathematical model	13
3.2 Analysis of the electron release probability	17
3.3 About LiF:Mg,Ti	20
4 Simulations	22
4.1 Materials used for simulations	22
4.2 Simulations	22
5 Results	26
5.1 Irradiation	26
5.2 Relaxation	28
5.3 Heating	31
Conclusiones	35
Conclusions	37
Bibliography	39

Index of Figures

- 3.1 Fermi-Dirac distribution $f(E)$ plotted against energy for different temperatures (0.1 K, 300 K and 600 K) at four key stages of the thermoluminescence process: (a) Before irradiation, where electrons follow a standard Fermi-Dirac distribution centered at the Fermi Level E_F ; (b) After irradiation, the system develops separate quasi-Fermi levels for electrons (E_{Fe}) and holes (E_{Fh}), deforming the previous distribution; (c) During stimulation, where thermal effects shift both quasi-Fermi levels closer to equilibrium, and the distribution approaches the original shape; (d) Final equilibrium, where the system returns to a standard Fermi-Dirac distribution with the Fermi Level E_F restored. 14
- 3.2 Jabłoński diagram of the theoretical model for the thermoluminescence process. The energy is situated in the Y axis, and the different components of the system are shown: traps (p_k : electron release probability, A_k : recombination probability, N_k : total density of available positions), recombination centers ($^h p_j$: hole excitation probability, A_j : electron trapping probability, $^j A_{mn}$: electron recombination probability), and the conduction (B.C) and valence (B.V) bands with the respective electron-hole pair generation rate (G). 14
- 3.3 Experimental thermoluminescence glow curve of LiF:Mg,Ti showing the emitted light intensity [u.a] plotted against temperature (°C). The most prominent is the main dosimetric peak around 200 °C, which is stable and reproducible. Lower-temperature peaks (<150 °C) correspond to shallow traps with poor thermal stability, while intermediate peaks (150–200 °C) suggest more complex trapping mechanisms. The measurement reflects the material's characteristic response following exposure to ionizing radiation. 21
- 5.1 Evolution of trap concentrations $n_i(t)$ plotted against time for the LiF:Mg, Ti during the irradiation phase for both models (a) Temperature dependent model, where the probabilities of excitation vary with temperature; (b) Temperature independent model, where the excitation probabilities are fixed parameters. Both were subjected to a constant irradiation rate of $G = 1000 \text{ cm}^{-3} \text{ s}^{-1}$ and a laboratory temperature of $T = 25 \text{ }^\circ\text{C}$ during 3600 seconds. The traps are labeled as follows: I (blue), II (orange), III (green), IV (red), V (purple), and s (brown). 27

5.2 Recombination rates during the irradiation phase for both models. (a) Temperature-dependent model; (b) Temperature-independent model. The plotted quantities correspond to the radiative (dm_R/dt) and non-radiative (dm_{NR}/dt) recombination rates. Both models were subjected to a constant irradiation rate of $G = 1000 \text{ cm}^{-3} \text{ s}^{-1}$ and a laboratory temperature of $T = 25^\circ\text{C}$ during 3600 seconds.	27
5.3 Charge neutrality ratio for the LiF:Mg, Ti plotted against temperature during the irradiation phase for both models. (a) Temperature dependent model; (b) Temperature independent model. The plotted ratio corresponds to the total negative charge divided by the total positive charges in the system. Both simulations were performed under a constant generation rate of $G = 1000 \text{ cm}^{-3} \text{ s}^{-1}$ and a laboratory temperature of $T = 25^\circ\text{C}$ during 3600 seconds.	28
5.4 Evolution of trap concentrations $n_i(t)$ plotted against time for the LiF:Mg, Ti during the relaxation phase for both models (a) Temperature dependent model; (b) Temperature independent model. Both were subjected to a constant generation rate of $G = 0 \text{ cm}^{-3} \text{ s}^{-1}$ and a laboratory temperature of $T = 25^\circ\text{C}$ during 604,800 seconds. The traps are labeled as follows: I (blue), II (orange), III (green), IV (red), V (purple), and s (brown).	29
5.5 Recombination rates for the LiF:Mg, Ti during the relaxation phase for both models. (a) Temperature dependent model; (b) Temperature independent model. The plotted quantities correspond to the radiative (dm_R/dt) and non-radiative (dm_{NR}/dt) recombination rates. Both models were subjected to a constant generation rate of $G = 0 \text{ cm}^{-3} \text{ s}^{-1}$ and a laboratory temperature of $T = 25^\circ\text{C}$ during 604,800 seconds.	30
5.6 Charge neutrality ratio for the LiF:Mg, Ti plotted against temperature during the relaxation phase for both models. (a) Temperature dependent model; (b) Temperature independent model. The plotted ratio corresponds to the total negative charge divided by the total positive charges in the system. Both simulations were performed under a constant generation rate of $G = 0 \text{ cm}^{-3} \text{ s}^{-1}$ and a laboratory temperature of $T = 25^\circ\text{C}$ during 604,800 seconds.	31
5.7 Evolution of trap concentrations $n_i(t)$ for the LiF:Mg, Ti plotted against temperature during the heating phase for both models. (a) Temperature dependent model; (b) Temperature independent model. For each trap, both the activation temperature (filled circle) and peak temperature (star icon) are indicated. The peak temperature has a dotted line that reaches the X axis and indicates the specific value for each trap. The simulations were performed under a constant generation rate of $G = 0 \text{ cm}^{-3} \text{ s}^{-1}$ and an increasing laboratory temperature from 0°C to 400°C during 400 seconds. The traps are labeled as follows: I (blue), II (orange), III (green), IV (red), V (purple), and s (brown).	32

- 5.8 Thermoluminescence (TL) glow curves for the LiF:Mg,Ti material plotted against temperature during the heating phase for both models. (a) Temperature dependent model; (b) Temperature independent model. The curves correspond to the radiative recombination rate dm_R/dt , showing the intensity of light emitted as trapped carriers recombine. For each visible peak, both the activation temperature (filled circle) and the peak temperature (star icon) are indicated. A vertical dotted line extends from each peak temperature to the X-axis, where the temperature value is labeled. The simulations were performed under a constant generation rate of $G = 0 \text{ cm}^{-3} \text{ s}^{-1}$ and an increasing laboratory temperature from 0 °C to 400 °C during 400 seconds. The traps are labeled as follows: I (blue), II (orange), III (green), IV (red), V (purple), and s (brown). 33
- 5.9 Charge neutrality ratio for the LiF:Mg, Ti plotted against temperature during the heating phase for both models. (a) Temperature dependent model; (b) Temperature independent model. The plotted ratio corresponds to the total negative charge divided by the total positive charges in the system. Both simulations were performed under a constant generation rate of $G = 0 \text{ cm}^{-3} \text{ s}^{-1}$ and an increasing laboratory temperature from 0 °C to 400 °C during 400 seconds. 34

List of Tables

3.1 Energies for the different traps and recombination centers in LiF:Mg,Ti. E_t represents the thermal energy, E_{ph} the phonon energy, and E_0 the total energy threshold.	18
4.1 Kinetic and structural parameters used in the simulations. Each trap and recombination center is characterized by its activation energy (E_i), frequency factor (s_i), electron trapping probability factor (A_i), and total density of electrons (N_i). The values are based on experimental data for LiF:Mg,Ti.	23

Resumen

Este trabajo supone la simulación y el análisis de un modelo matemático que describe la respuesta termoluminiscente (TL) del LiF:Mg, Ti; un material ampliamente utilizado en la dosimetría de radiación. Los procesos físicos subyacentes a este fenómeno se han traducido en un conjunto de ecuaciones diferenciales, y de ahí se han desarrollado dos modelos; uno con un factor de frecuencia constante y otro con un factor de frecuencia que depende de la temperatura, cuya dependencia está fundamentada en los principios de la física estadística cuántica.

El entorno de la simulación, construído en Python, resuelve numéricamente el sistema de ecuaciones diferenciales para las tres fases clave de la termoluminiscencia: irradiación, relajación y calentamiento. Ambos modelos reproducen con éxito la curva termoluminiscente característica para el LiF:Mg, Ti vista en los datos experimentales, pero el modelo dependiente de la temperatura consigue una descripción más precisa de las trampas poco profundas. Este modelo muestra que la trampa I presenta una saturación más temprana, una mayor liberación termina y un cambio en la posición e intensidad de los picos en comparación con el modelo independiente de la temperatura. Las trampas más profundas (de II a V) muestran una variación menor entre ambos modelos, lo que sugiere que su comportamiento es menos sensible a la diferencia en la expresión del factor de frecuencia.

Las curvas termoluminiscentes simuladas reproducen los cinco picos característicos del LiF:Mg, Ti observados en los datos experimentales. La concordancia entre la temperatura pico y los máximos de la curva termoluminiscente refuerza la validez del modelo. Este trabajo no solo reproduce el comportamiento conocido de la TL del LiF:Mg, Ti, sino que también destaca la importancia de la dependencia de la temperatura en el factor de frecuencia, ya que mejora la capacidad del modelo para explicar la dinámica de los portadores de carga. Un trabajo futuro podría afinar aún más este modelo incorporando una dependencia de la temperatura más compleja.

Palabras clave: Termoluminiscencia; LiF:Mg, Ti; Radiación; Dosimetría; Simulación

Abstract

This work presents the simulation and analysis of a mathematical model for the thermoluminescent (TL) response of LiF:Mg, Ti; a material widely used in radiation dosimetry. The physical processes underlying thermoluminescence were drawn through a set of differential equations, and two models were developed: one with a constant frequency factor and another with a temperature dependent frequency factor based on quantum statistical mechanics.

The simulation environment, built in Python, numerically solved the differential equations for the three key phases of the TL process: irradiation, relaxation, and heating. Both models successfully reproduce the characteristic TL glow curve of LiF:Mg, Ti, but a more accurate representation of shallow traps is achieved with the temperature dependent model. This model shows that trap I exhibits earlier saturation, greater thermal release, and a shift in peak position and intensity compared to the temperature independent model. Deeper traps (II to V) showed minimal variation between models, suggesting that their behavior is less sensitive to the difference in the frequency factor's expression.

The simulated TL glow curves reproduced the characteristic five peaks of LiF:Mg, Ti shown in experimental data. The agreement between the peak temperature and the glow curve maxima reinforces the model's validity. This work not only reproduces the known TL behavior of LiF:Mg, Ti but also highlights the significance of temperature dependency in the frequency factor, enhancing the model's ability to explain charge carrier dynamics. Future work may refine this model further, potentially incorporating more complex temperature dependencies.

Keywords: Thermoluminescence; LiF:Mg, Ti; Radiation; Dosimetry; Simulation

CHAPTER 1

Introduction

As a bystander, one may pass life without thinking of the things that surrounds us. One may have had the misfortune of entering on an MRI, or the responsibility to carry a dosimeter in a nuclear plant, and stepped out the room as it is. Life can go on unquestioned, and one may get out of that PET scan without thinking of the source of that awful noise.

There's beauty in the mundane, and the world is full of wonders. The universe is a complex system of interactions, and we know a very small part of it. We are surrounded by radiation, and we are constantly exposed to it. It is a natural phenomenon that has been present since the beginning of time, and it is an integral part of our existence. There are answers for those who wonder, and this work is a very small step towards it.

Luminescence is a phenomenon familiar to us; and goes through our lives like a commercial break. We see it in the glow of a firefly, the sparkle of a diamond, or the light emitted by a fluorescent lamp. In a nutshell, it is a process where energy is absorbed and re-emitted as light, leaving a trail behind, and can be triggered by various stimuli, like heat, light or radiation. This broad notion is the reason why the study of luminescence has practical uses in many fields. One of those fields of use is the detection of ionizing radiation, a field generally known as "dosimetry". The amount of radiation absorbed by a material can be measured by the amount of light emitted when the material is stimulated, and this is the basis for many dosimetry techniques. These luminescence-based methods for detecting ionizing radiation have played a central role in radiation research since the earliest discoveries of radiation, as they exploit the ability of specific materials to emit light when exposed to ionizing radiation, to detect and quantify the radiation received, further expanding the knowledge its efect.

One of the most commonly used materials in this context is lithium fluoride doped with magnesium and titanium ($\text{LiF}:\text{Mg,Ti}$). This material exhibits thermoluminescence, a phenomenon where after irradiation, its internal structure captures a memory of the event, in the form of trapped electrons. Upon heating, these trapped charges are released; recombining and emitting photons in the process. The resulting light —that we know to be called luminescence—, if recorded as a function of temperature, produces what is called a thermoluminescence (TL) glow curve.

But knowing that LiF:Mg,Ti emits light when heated is only the beginning. The real challenge lies in understanding it. Interpreting it. The glow curve, with its peaks and valleys, is more than a passive result. It is a message from within the material, shaped by the dance of the electrons across the imperfections of the lattice, and it tells a story—if we know how to read it.

To make sense of that story, one must model it. That is, to simulate the physical processes that give rise to the observed glow, and to see whether our mathematical model truly mirror nature. Can we, with a set of parameters and approximations, recreate the fingerprint of radiation? Can we extract from that curve a clear image of the processes within?

This is where this work begins. At the heart of this discourse lies the attempt to reproduce the TL glow curve of LiF:Mg,Ti through computational modeling. This effort leans on the shoulders of many brilliant scientists with an insatiable hunger for one of the many mysteries of the universe, one where electrons takes us across energy barriers, where recombination is probabilistic, and where heat becomes the catalyst of understanding.

But even the best models are incomplete. Many assume constant parameters—fixed frequency factors and activation energies, unchanged by temperature or entropy. Reality, as often, lies in a space in between. In these pages, it will be investigated what happens when we let these parameters breathe. By introducing temperature-dependent frequency factors, we will investigate how this modification reshapes the predicted glow curve. Is the model improved? Do we get closer to the experimental results? Can it go beyond known data and predict a hypothetical future case?

Ultimately, the motivation is simple: to understand. To refine our lens on thermoluminescence; to bridge the gap between theory and experience, and to contribute, even in the smallest way, to the slow unraveling of the invisible questions that shape our everyday lives.

CHAPTER 2

Objectives

The aim of this work is to study the thermoluminescent (TL) behavior of LiF:Mg,Ti through a computational simulation of the physical processes involved. Based on the mathematical model presented in Chapter 3, the objective is to numerically solve the system of differential equations that describe the dynamics of the TL process during the three key phases: Irradiation, Relaxation and Heating. For that, two mathematical models have been developed, one that follows the general practice in the field used as reference, often referred to as the *temperature independent model*, and one that dives deeper into the physics of the process and considers a further role on the temperature dependence of its parameters, referred to as the *temperature dependent model*.

The specific objectives of this work are:

- 1. Develop a mathematical model** that describes the thermoluminescent behavior of LiF:Mg,Ti, based on the physical processes involved in the TL phenomenon. For that, it will be important to understand the fundamental mechanisms of ionic crystals, the role of impurities, and the processes of electron trapping and recombination that ultimately leads to the emission of light.
- 2. Implement and validate a numerical method** to solve the system of differential equations derived from the mathematical model, allowing for the simulation of the TL process. Using a set of physically accurate parameters, the models should be able to reproduce the characteristic TL glow curves observed in experimental data, and be capable of tracing back the evolution of the system to its initial state.
- 3. Analyze and compare the results of both models** to understand the impact of temperature dependence on the TL behavior of LiF:Mg,Ti. One of the central objectives of this work is to determine how the temperature dependence affects the shape and intensity of the TL glow curves and whether both models yield similar results under certain conditions, and ultimately reproduce a similar behavior to the one observed in experimental data.
- 4. Interpret the simulated thermoluminescent signal** to draw conclusions about the physical processes involved in the TL phenomenon. The final goal is to obtain the TL glow curve from the simulated heating phase and extract from it key information

such as the activation and peak temperatures for each trap. This will allow for a deeper understanding of the trapping and recombination processes in LiF:Mg,Ti, and how they are influenced by temperature.

Ultimately, this study aims not only to reproduce the characteristic behavior of LiF:Mg,Ti through simulation, but also to question about the physics behind the interactions of the particles involved. By comparing different approximations made into models, this work contributes to a better understanding of how different theoretical assumptions can reach a similarity with the experimental truth.

CHAPTER 3

Theoretical framework

3.1. THE MATHEMATICAL MODEL

To describe the thermoluminescent response of a semiconductor, we can use a mathematical model based on the trapping and releasing of charge carriers in the accessible energy levels of the material.

Let us first consider the case of an arbitrary semiconductor without impurities. The energy levels of the conduction band and the valence band are separated by a bandgap E_g , and can be obtained with Schrodinger's equation that is under the influence of a periodic potential:

$$\left[-\frac{\hbar^2}{2m} \nabla^2 + V(\vec{r}) \right] \psi(\vec{r}) = E \psi(\vec{r}), \quad (3.1)$$

The periodicity of the potential $V(\vec{r})$ for any lattice vector \vec{R} allows the Bloch's theorem to apply, and so it gives rise to the formation of a band structure, composed by the conduction band, which is typically fully occupied at absolute zero temperature, and the valence band, which is in turn typically empty -or rather, we can consider it filled with holes (h^+), or "positively charged electrons". The bandgap E_g is then defined as the energy difference between the top of the valence band and the bottom of the conduction band, and for a perfect crystal, no energy states are allowed in that region. This can be clearly seen if we take into account the density of available states, $D(E)$, which is a function of the Fermi-Dirac distribution $f(E)$ for a certain temperature T . This function gives the occupancy of any energy level E , and can be expressed as:

$$f(E) = \frac{1}{e^{\frac{E-E_f}{k_B T}} + 1}, \quad (3.2)$$

Where E_f is the Fermi Level, and k_B is the Boltzmann constant. If the system is in equilibrium, and we set the case of $T = 0K$, the occupancy function $f(E)$ will be equal

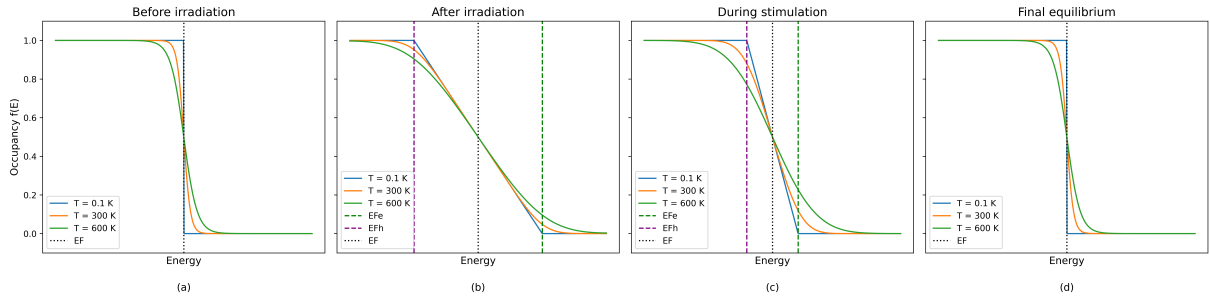


Figure 3.1: Fermi-Dirac distribution $f(E)$ plotted against energy for different temperatures (0.1 K , 300 K and 600 K) at four key stages of the thermoluminescence process: (a) Before irradiation, where electrons follow a standard Fermi-Dirac distribution centered at the Fermi Level E_F ; (b) After irradiation, the system develops separate quasi-Fermi levels for electrons (E_{Fe}) and holes (E_{Fh}), deforming the previous distribution; (c) During stimulation, where thermal effects shift both quasi-Fermi levels closer to equilibrium, and the distribution approaches the original shape; (d) Final equilibrium, where the system returns to a standard Fermi-Dirac distribution with the Fermi Level E_F restored.

to 1 for all energy levels below the Fermi level, and 0 for all energy levels above it. This means that the occupancy function will be a step function, with a discontinuity at the Fermi level, and so we can see that there are no available states in the bandgap region.

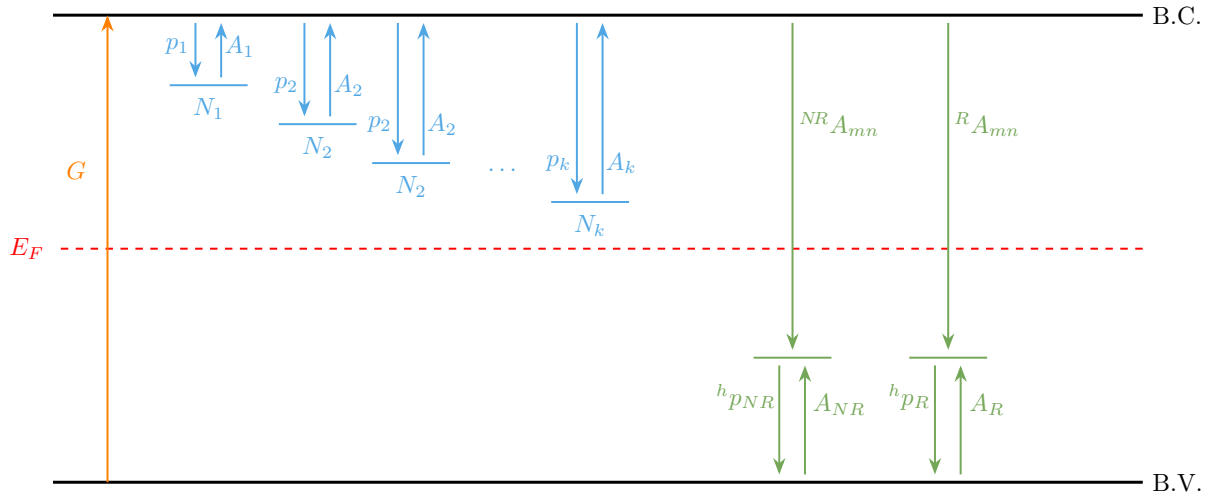


Figure 3.2: Jabłoński diagram of the theoretical model for the thermoluminescence process. The energy is situated in the Y axis, and the different components of the system are shown: traps (p_k : electron release probability, A_k : recombination probability, N_k : total density of available positions), recombination centers (${}^h p_j$: hole excitation probability, A_j : electron trapping probability, ${}^j A_{mn}$: electron recombination probability), and the conduction (B.C) and valence (B.V) bands with the respective electron-hole pair generation rate (G).

The introduction of impurities or defects however, break the periodicity of the lattice, and create localized energy levels inside this “forbidden region”. These levels can be thought of as traps for electrons if we are situated above the fermi level, and traps of holes

if we are situated below. When this material is irradiated, electrons from the valence band can be excited to the conduction band, creating an electron-hole pair; and so changing the shape of the occupancy function. Once excited, both electrons and holes get “trapped” in these localized energy levels, and the excitation of these pairs into equilibrium will result in the emission of energy. In Figure 3.1 we can see a broad description of the perturbation of the system from its equilibrium state due to the irradiation, and the return of the system to equilibrium during either thermal stimulation or optical stimulation. If said relaxation processes are radiative, TL and OSL result.

And so, we can see a schematic representation of our theoretical model in Figure 3.2. Situating the energy in the Y axis, the focus is set in the energy gap of our material. Drawn as a blue or green horizontal line are the energy traps; in blue above the Fermi level there are electron traps, and in green there are hole traps or recombination centers. The vertical arrows describe available transitions; the ones pointing upwards represent an excitation process, and the ones pointing downwards represent a relaxation process.

Mathematically, we can describe these processes with a set of differential equations that take into account the rate of change of the number of electrons and holes in the bands and traps. This set will depend on the properties of the material, and the luminescence response we are trying to model. For an arbitrary system, we can write the following set of equations that describe the rate of change of the number of electrons and holes in the conduction band n_c , the valence band n_v :

$$\frac{dn_c}{dt} = \textcolor{blue}{G} - \left[\sum_i \frac{dn_i}{dt} \right] \cdot n_c - \left[\sum_{j=R,NR} {}^i A_{mn} \cdot m_j \right] \cdot n_c \quad (3.3)$$

$$\frac{dn_i}{dt} = -p_i \cdot n_i + A_i \cdot [N_i - n_i] \quad (3.4)$$

$$\frac{dm_j}{dt} = -{}^h p_j \cdot m_j + A_j \cdot [M_j - m_j] \cdot n_v - {}^i A_{mn} \cdot m_j \cdot n_c \quad (3.5)$$

$$\frac{dn_v}{dt} = \textcolor{blue}{G} - \sum_{j=R,NR} [-{}^h p_j \cdot m_j + A_j \cdot [M_j - m_j] \cdot n_v] \quad (3.6)$$

Where every term is defined as follows:

- G : electron-hole pairs generation rate by the radiation [$\text{cm}^{-3} \text{ s}^{-1}$]
- n_c : electron concentration in the conduction band [cm^{-3}]
- n_v : electron concentration in the valence band [cm^{-3}]
- n_i : electron concentration in trap i [cm^{-3}]
- m_j : hole concentration in the recombination center j [cm^{-3}]
- N_i : total density of available positions in electron trapping centres in trap i [cm^{-3}]
- M_j : total density of available positions in recombination centers [cm^{-3}]
- p_i : electron release probability factor for trap i [s^{-1}]
- ${}^h p_j$: hole release probability factor for recombination center j [s^{-1}]

- A_i : electron trapping probability factor for trap i [$\text{cm}^3 \text{ s}^{-1}$]
- ${}^i A_{mn}$: recombination probability factor for recombination center j [$\text{cm}^3 \text{ s}^{-1}$]

Equation 3.3 describes the change rate of electron concentrations in the conduction band. To interpret this equation, we can see that to the electron-hole pairs generated by the radiation (G), there are two terms subtracted. The first one correlates to the electrons that leave the continuum levels of the conduction band and get trapped in the discrete levels of the material —a process described by 3.4, that will have a further discussion in section 3.2—, and the second one answers to the electrons in the conduction band that recombine with holes with a radiative (R) or non-radiative (NR) process. It is easy to see that this second term corresponds to the third term of 3.5.

The change rate of electron concentrations in the valence band is shown in 3.6, and it follows a similar logic. This time however, we only take into account the terms multiplied by the electron density in the valence band (n_v) seen in equation 3.5; one that represents the holes leaving the continuum to get trapped in the recombination centers, and another that accounts for the addition of electrons that are released from the recombination centers and recombine with the holes in the valence band. The terms described correspond to Equations 3.4 and 3.5 describe the total change rate of electrons and holes in the discrete levels of the material. The signs of the terms in these equations follow the convention that we are set in the conduction band, and so any electron that leaves the conduction band is represented with a negative term, and any electron that enters is represented with a positive term.

To carry out a numerical simulation of the process, we will need to solve the set of differential equations 3.3 – 3.6 using RKF-45 method, which is a Runge-Kutta method of order 4 and 5. This method will obtain the charge concentration in all traps and recombination centers at an instant of time. The solving of this set of equations will be done for the three phases required to obtain the TL glow curve. To do this, the intrinsic and kinetic parameters are kept constant, varying the external conditions of the system such as temperature and electron-hole pair generation rate.

The first phase is *irradiation*, where the material is exposed to ionizing radiation. It begins with all levels initially empty [$n_c(0) = n_v(0) = n_i(0) = m_j(0) = 0$], and the electron-hole pairs generated as a result will have a constant value as a function of time ($G = 1000 \text{ cm}^{-3} \text{ s}^{-1}$). The temperature is set to a constant $T = 25 \text{ }^\circ\text{C}$ and the filling process takes one hour (3600 seconds). The second phase is *relaxation*, where the material is left undisturbed at a constant temperature for a defined period of time. Taking as initial values the final values of the irradiation phase, the temperature is kept constant at $T = 25 \text{ }^\circ\text{C}$, and the electron-hole pairs generation rate is set to $G = 0 \text{ cm}^{-3} \text{ s}^{-1}$. The relaxation process is set for one week (604,800 seconds). Finally, the third phase is *heating*, where the material is taken from an initial temperature T_0 to a final temperature at a constant linear heating rate during 400 seconds. The numerical resolution of the set equations is similar to the previous phases, but now with the temperature varying linearly with the expression:

$$T(t) = T_0 + \beta \cdot t \quad (3.7)$$

Where the heating rate is set to $\beta = 1 \text{ }^\circ\text{C s}^{-1}$. The electron-hole pairs generation rate is set to $G = 0 \text{ cm}^{-3} \text{ s}^{-1}$, and the charge concentration values are taken from the final values

of the relaxation phase. The heating process is set to last 400 seconds. The results after the numerical resolution of the set of equations will be the charge concentration values for every instant of time throughout the whole heating cycle $[n_c(t), n_v(t), n_i(t), m_j(t)]$. It is in this phase when the luminescent emission occurs, and so the intensity of the emitted light can be estimated in relation to the radiative recombination of electron-hole pairs. We can give the expression for the intensity of the emitted light as it follows:

$$I_{TL}(t) = -\frac{dm}{dt} \approx {}^R A_{mn} \cdot m_R \cdot n_c \quad (3.8)$$

We can write this dependence as a function of temperature by:

$$I_{TL}(t) = -\frac{dm}{dt} = -\frac{dm}{dt} \cdot \frac{dT}{dT} = -\frac{dm}{dT} \cdot \frac{dT}{dt} = -\frac{dm}{dT} \cdot \beta = I_{TL}(T) \cdot \beta \quad (3.9)$$

Representing this intensity as a function of temperature will be the objective of the simulations, as it is the key to understand the thermoluminescent response of the LiF:Mg,Ti after being irradiated.

3.2. ANALYSIS OF THE ELECTRON RELEASE PROBABILITY

As introduced in Section 3.1, there is a greater discussion to be had about the releasing probability of electrons and holes, as it determines in great part the electron-hole pairs available to recombine. In general, two distinct mechanisms may contribute to the release of a trapped carrier: *thermal* and *optical (photo)excitation*. In the first one, the electron gains sufficient energy from lattice vibrations to overcome the trap depth, and in the latter the release is induced by the absorption of a photon whose energy exceeds the one binding the carrier to the trap. An electron trapped in a lattice defect with energy E_t and temperature T will have a probability of being released that is the result of:

$$p = p_{th} + p_{ph} \quad (3.10)$$

Where p_{th} is the thermal excitation probability and p_{ph} is the optical excitation probability. The thermal contribution follows Arrhenius equation. The probability per second that the electron will be thermally excited into the conduction band is given by:

$$p_{th} = s \cdot e^{-\frac{E_t}{k_B T}} \quad (3.11)$$

Where s is known as the *frequency factor* [s^{-1}]. It can be interpreted as the “attempt to escape” frequency, as it is a measure of the number of times per second that energy is absorbed from phonons in the lattice. The exponential that follows is the probability that the energy absorbed is enough to cause a transition from the localized state to the conduction band. For the optical contribution on the other hand, the trapped electrons are released from their traps via absorption of energy from photons [1], and the probability is given by:

$$p_{ph} = \sigma_P(E) \cdot \Phi \quad (3.12)$$

Where $\sigma_P(E)$ is the photoionization cross-section [cm^2], which is a measure of the

probability that a photon with energy E will be absorbed by an electron trapped in a lattice defect, and Φ is the photon flux or intensity of the stimulating light [$\text{cm}^{-2} \text{ s}^{-1}$], which is the number of photons per unit area per unit time. This process is particularly relevant in optically stimulated luminescence (OSL), where the material is stimulated with light to release the trapped electrons and produce a luminescent signal. If E_0 is the threshold photon energy required to excite the electron from the trap, instead of considering only the thermal trap depth E_t as one may expect, we should initially consider the effect of the contribution of lattice phonons such that:

$$E_0 = E_t + E_{ph} \quad (3.13)$$

Where E_{ph} is given by:

$$E_{ph} = S_{HR} \cdot h \cdot \nu_{ph} \quad (3.14)$$

And here S is the Huang-Rhys factor, which is a dimensionless parameter that characterizes the degree of electron-phonon coupling in a luminescent material that usually ranges on the order of 1–2 [10]. The higher the Huang-Rhys factor, the stronger the electron-phonon coupling, and so the greater the energy shift of the trap level due to lattice vibrations. The term $h \cdot \nu_{ph}$ is the energy of a phonon with frequency ν_{ph} [s^{-1}], where h is Planck's constant [$\text{eV} \cdot \text{s}$]. For LiF the phonon frequency is typically around 900 cm^{-1} [7], which corresponds to a phonon energy of approximately 0.11 eV. If we take a Huang-Rhys factor of $S_{HR} = 1$, we can estimate the energy shift given a set of experimental values for the thermal energies E_t of the traps. The results are shown in 3.1 and with them we see that the energy threshold E_0 is primarily determined by the thermal trap depth E_t , with the phonon energy E_{ph} contributing a small correction.

Table 3.1: Energies for the different traps and recombination centers in LiF:Mg,Ti. E_t represents the thermal energy, E_{ph} the phonon energy, and E_0 the total energy threshold.

Parameters		E_t (eV)	E_{ph} (eV)	E_0 (eV)
Trapping Centers	Trap I	1.19	0.11	1.30
	Trap II	1.60	0.11	1.71
	Trap III	1.76	0.11	1.87
	Trap IV	1.87	0.11	1.98
	Trap V	1.98	0.11	2.09
Recombination centers	Trap s	2.70	0.11	2.81
	Radiative	2.30	0.11	2.41
	Non Radiative	2.30	0.11	2.41

This observation reinforces the suitability of studying the thermoluminescence (TL) independently of optically stimulated luminescence (OSL). The fact that the thermal energy E_t stays over zero confirms that thermal energy alone is sufficient to release charge carriers from traps over a physically accessible temperature range. Furthermore, in TL

measurements, no external optical stimulation is applied during readout, and so the photon flux in a darkened environment is negligible. As a result, photo-induced excitation does not contribute meaningfully to the observed luminescence signal. From now on, we will close our focus on the thermoluminescence process, and so we will only consider the thermal excitation probability p_{th} in our simulations.

If we aim to deepen our understanding of equation 3.11, we can look a little further in the concept of the frequency factor s . It is a crucial parameter in the study of thermoluminescence, as it determines the rate at which electrons are released from traps. It is a function of the material properties, as shown in its definition:

$$s = \nu_{ph} \cdot K \cdot e^{\frac{\Delta S}{k_B}} \quad (3.15)$$

Where ν_{ph} is the lattice phonon vibration frequency and K is the transition probability constant, that takes the value 0 or 1 depending on whether the transition is allowed or forbidden. Typically, one can expect $s \sim 10^{12} - 10^{14} \text{ s}^{-1}$, which is consistent with the values of ν for most solids. The term $e^{\Delta S/k_B}$ is a correction factor that accounts for the entropy change associated with the transition from the localized state to the conduction band.

From equation 3.15 we see that the frequency factor has an exponential dependency with the entropy change. This, taking the Quantum Statistical Mechanics theory [3], does not align with the invariance of said factor with temperature, as entropy, with its own definition, should vary when temperature does. While a rigorous proof of the overall temperature dependence of the frequency factor is beyond the scope of this work, one model is proposed to provide an approximate perspective on how this dependency could influence the resulting TL glow curve.

At first glance, the simplest model was considered, where the entropy would be linear with the temperature ($\Delta S \propto T$). This theory was quickly discarded as would make the entropy factor increase exponentially with the temperature ($s \propto e^T$), and so the probability of excitation would tend to infinity in a very short range of temperature increase.

To solve this issue, a more refined model was considered, where the entropy would now be logarithmically dependent on the temperature ($\Delta S \propto \ln(T)$). The constant of the proportionality could be called α , and so the resulting expression of the frequency factor can be written as:

$$s = \nu_{ph} \cdot K \cdot T^{\alpha/k_B} \quad (3.16)$$

It is clear now that a softer dependency with the temperature is achieved, and the previous problem of the entropy factor tending to infinity is solved. The value of α can be adjusted to keep the entropy contribution at a realistic magnitude —typically we have $\Delta S \sim 1-3 \text{ } k_B$ over the glow curve temperature range—. For that reason, we have selected a value of:

$$\alpha = \frac{1.5 \text{ } k_B}{\ln(300)} \approx 0.26 \text{ } k_B \quad (3.17)$$

This choice ensures that the frequency factor remains within a reasonable range across

the temperature spectrum of interest, and yields TL glow curves that are consistent with experimental observations of LiF:Mg,Ti materials.

3.3. ABOUT LiF:Mg,Ti

Lithium fluoride (LiF) is a crystalline material that has been widely used in radiation dosimetry due to its favorable properties. It first appeared as a thermoluminescent dosimetry material in the 1950's, and since then, it has been extensively studied in the field of radiation detection. The material is composed of lithium (Li) and fluor (F) atoms, forming a crystal lattice structure of a face-centered cubic (FCC) type. Without any impurities, LiF is a semiconductor, with a bandgap of approximately 14 eV, which makes it an excellent insulator at room temperature.

To enhance the properties for radiation detection, LiF is often doped with magnesium (Mg) and titanium (Ti) ions, and sold commercially as TLD-100 [5]. The doping process introduces defects in the crystal lattice, creating energy levels within the bandgap. These defects play a crucial role in trapping and releasing charge carriers, which are responsible for the thermoluminescent response of the material. This process is known as thermoluminescence (TL), where the trapped electrons are released upon heating, resulting in the emission of light. The intensity of this emitted light is proportional to the amount of radiation absorbed by the material, making it a valuable tool for dosimetry.

The TL response of LiF:Mg,Ti is characterized by a glow curve, which is a plot of the intensity of emitted light as a function of temperature. The glow curve typically exhibits several peaks, each corresponding to different trapping levels in the material. The position and shape of these peaks can provide valuable information about the trapping and recombination processes occurring in the material, and they are key to understanding the thermoluminescent response of LiF:Mg,Ti. In Figure 3.3 we can see an experimental glow curve of LiF:Mg,Ti plotted with data provided by the Radiation Dosimetry Laboratory of CIEMAT, which shows a typical response with several peaks at different temperatures.

This characteristic shape of the glow curve for LiF:Mg,Ti has been extensively documented [1] [4] [6], and it is a result of the specific energy levels introduced by the doping process, with the main peak typically occurring around 200 °C. Each peak arises from the thermal release of electrons from traps of different activation energies, if followed by recombination in the recombination centers. The graph shows the luminescence intensity plotted against temperature, and reveals five distinct glow peaks. Each of those peaks corresponds to the thermal release of trapped charge carriers from specific trap levels, and their height and position can be crucial to determine the trap depth and recombination probability. They can be categorized into:

- **Main dosimetric peak (~ 200 °C).** It has the most favorable characteristics for dosimetry: high intensity, good linearity with dose, and appears consistency at the same temperature, which helps to exhibit good reproducibility across different measurements and a relatively simple kinetic behavior. It is thermally stable at room temperature for long periods of time, meaning their signal do not fade significantly over days or weeks.

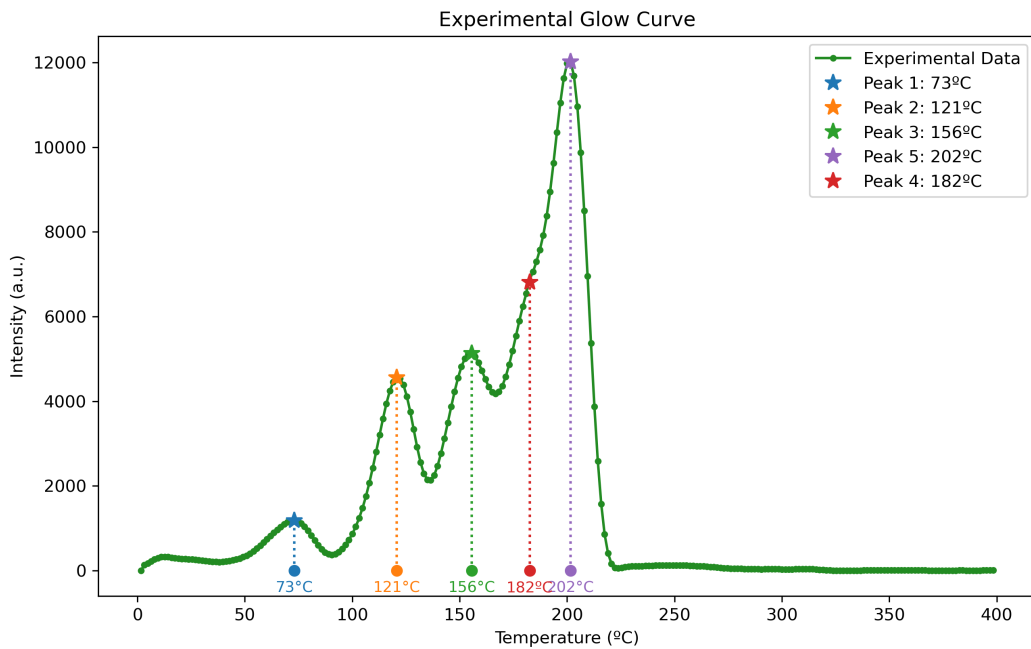


Figure 3.3: Experimental thermoluminescence glow curve of $\text{LiF}: \text{Mg}, \text{Ti}$ showing the emitted light intensity [a.u] plotted against temperature ($^{\circ}\text{C}$). The most prominent is the main dosimetric peak around $200\text{ }^{\circ}\text{C}$, which is stable and reproducible. Lower-temperature peaks ($< 150\text{ }^{\circ}\text{C}$) correspond to shallow traps with poor thermal stability, while intermediate peaks ($150\text{--}200\text{ }^{\circ}\text{C}$) suggest more complex trapping mechanisms. The measurement reflects the material's characteristic response following exposure to ionizing radiation.

- **Lower-temperature peaks ($< 150\text{ }^{\circ}\text{C}$).** They are associated with shallower traps, and are thermally less stable at ambient conditions. They tend to fade significantly at room temperature over time—that is, undergo great signal loss due to thermal stimulation from room temperature alone—, and as a consequence, are not useful for dosimetric purposes. However, they are useful for fundamental studies of trapping and recombination processes, offering insight into the energy structure of the material and their mechanisms of carrier release.
- **Intermediate peaks (between $150\text{ }^{\circ}\text{C}$ and $200\text{ }^{\circ}\text{C}$).** As expected, they suppose a middle ground. These peaks represent a transitional region in trap stability and interaction complexity. They are believed to arise from more complex or composite trapping structures, possibly involving multiple trapping levels or interactions between traps and recombination centers and their intensity and position can shift or merge depending on the specific conditions of the sample, the dose or the thermal history. In some cases, peaks in this range can interfere with or overlap the main dosimetric peak, which can complicate deconvolution and dose evaluation.

CHAPTER 4

Simulations

4.1. MATERIALS USED FOR SIMULATIONS

The materials used for this work are all the digital tools required for the simulation of the behavior of our material of choice. In our case, the project was made using *Python* in a Jupyter Notebook. The programs written are available on the GitHub repository called `TFG_MartadelaRosa`.

The libraries used for the simulations are:

- `numpy`: This library is used for numerical calculations and array manipulations.
- `matplotlib`: This library is used for plotting graphs and visualizing data.
- `pandas`: This library is used for data manipulation and analysis, providing data structures like DataFrames.
- `scipy`: This library is used for scientific computing and includes functions for optimization, integration, interpolation, and more. In particular to solve the differential equations that describe the kinetics of the TL process.

4.2. SIMULATIONS

To compute a simulation of the TL process described in Section 3.1, after defining the parameters of the model, we need to solve the differential equations that describe the kinetics of the TL process. The equations are solved using the `odeint` function from the `scipy.integrate` library. The function takes as input the system of equations, the initial conditions, and the time points at which we want to evaluate the solution. The output is an array containing the values of the variables at each time point, which is then saved to their corresponding variables, used to plot the results. They are brought to life using the

`matplotlib` library, and for every resolution of the differential equations, we will present three graphs as the result.

The first step to perform the simulations is to define the parameters of the model. These parameters include the activation energy (E_i), the frequency factor (s_i), the electron trapping probability factor (A_i), and total density of electrons (N_i) for each trapping center, as well as the recombination centers. The parameters used in our case can be found in Table 4.1. The values of these parameters are based on experimental data [4] for the specific material being studied, in this case, LiF:Mg,Ti, and are proposed within the margin of error. Once the model parameters have been defined, the simulation proceeds by numerically solving the system of differential equations described in equations 3.3–3.6. As we mentioned, this is done by using `odeint` function from the `scipy.integrate` library. For each phase, the appropriate parameters and initial conditions are set to a general simulation function that returns the evolution of all charge concentrations.

Table 4.1: Kinetic and structural parameters used in the simulations. Each trap and recombination center is characterized by its activation energy (E_i), frequency factor (s_i), electron trapping probability factor (A_i), and total density of electrons (N_i). The values are based on experimental data for LiF:Mg,Ti.

Parameters		E (eV)	s (s^{-1})	A ($\text{cm}^3 \text{s}^{-1}$)	N (cm^3)
Trapping Centers	Trap I	1.19	$1.00 \cdot 10^{15}$	10^{-8}	10^{10}
	Trap II	1.60	$1.41 \cdot 10^{14}$	10^{-8}	10^{10}
	Trap III	1.76	$9.05 \cdot 10^{15}$	10^{-8}	10^{10}
	Trap IV	1.87	$5.78 \cdot 10^{15}$	10^{-8}	10^{10}
	Trap V	1.98	$8.71 \cdot 10^{17}$	10^{-8}	10^{10}
	Trap s	2.70	$1.00 \cdot 10^{15}$	10^{-8}	10^{10}
Recombination centers	Radiative	2.30	$1.00 \cdot 10^{16}$	10^{-8}	10^{10}
	Non Radiative	2.30	$1.00 \cdot 10^{16}$	10^{-8}	10^{10}

To ensure modularity and consistency, the simulation is structured in reusable components. Each phase is simulated by calling the same solver function with different input values, and the output is automatically stored and passed between stages to maintain continuity. As two models have been used for the simulations, two separate functions were created to define the system of differential equations for the TL process. The first function, `diff_eqs_freqfactor()`, is used for the simulations of the TL process with a frequency factor that depends on the temperature following equation 3.16, while the second function, `diff_eqs_notemp()`, is used for the simulations where the frequency factor is a constant from Table 4.1. The functions take as input the current state of the system, the time, and the parameters of the model, and return the derivatives of the charge concentrations with respect to time. In the Listing 4.1, we can see the implementation of the first function for the irradiation phase of the TL process.

Listing 4.1: Python simulation of the irradiation phase in TL simulations. It defines the initial parameters, initializes trap and recombination center populations, solves the system of differential equations, and plots the results.

```

1 ## 2.1 IRRADIATION
2 # Parameters for IRRADIATION
3 value.kB = 8.617e-5          # Boltzmann constant (eV/K)
4 value.T_C = 25               # Temperature (celsius)
5 value.hr = 0                 # Heating rate (celsius/s)
6 value.G = 1000               # e-hole pair gen (cm-3 s-1)
7
8 # Time vector (s)
9 npoints = 3600
10 t = np.linspace(0, npoints-1, npoints)
11
12 # Initial conditions vector
13 n_I, n_II, n_III, n_IV, n_V, n_s = 0, 0, 0, 0, 0, 0
14 m_NR, m_R = 0, 0
15 n_c, n_v = 0, 0
16 y0 = [n_I, n_II, n_III, n_IV, n_V, n_s, m_NR, m_R, n_c, n_v]
17
18 # Solving the differential equations system
19 irradiation = odeint(diff_eqs_freqfactor, y0, t, args=(value,))
20 n_I, n_II, n_III, n_IV, n_V, n_s, m_R, m_NR, n_c, n_v
21     = irradiation.T
22
23 # Plotting the results
24 plot_results(irradiation, save_path, t, value)
25

```

After solving the system of differential equations for a given phase, the simulation outputs three diagnostic plots that represent the state and evolution of the material over time (or temperature in the case of the *heating* phase). These are:

- **Electron concentration $n_i(t)$ evolution:** This plot shows the temporal evolution in each trap. It provides insight into how the electron population in each trap changes over time, indicating the trapping and de-trapping processes. It shows how they are progressively filled with electrons during the irradiation phase, their stationary behavior in the relaxation phase, and their depletion during the heating phase. Their evolution depends on the parameters of each trap, and will have different shapes as a consequence.
- **Recombination rates:** The graph displays the rate of radiative (dm_R) and non-radiative (dm_{NR}) recombination processes as a function of time. It shows how the recombination rates change as the traps are filled and emptied. During irradiation, dm_R grows steadily as the traps fill up, to then drop rapidly to near zero during the relaxation phase, indicating that radiative recombination ceases once the irradiation stops and the system stabilizes in a metastable state. During heating, dm_R rises again as the trapped electrons are thermally released and recombine radiatively with holes, producing the TL glow peaks. It is in this graph for the heating phase when we expect to obtain our TL glow curve. Throughout all three phases, the non-radiative recombination rate (dm_{NR}) remains constant, confirming that non-radiative recombination plays an insignificant role in simulations.

- **Charge neutrality:** This plot shows the ratio of the total electron concentration to the total hole concentration as a function of time. It follows the expression:

$$\frac{n_c + n_I + n_{II} + n_{III} + n_{IV} + n_V + n_s}{m_R + m_{NR} + n_v} \approx 1 \quad (4.1)$$

And as such, it should be close to 1 throughout the simulation. This plot is useful to verify that the system remains charge neutral during the entire process, and can serve as a validity check to ensure that the simulation is correctly implemented. If the ratio deviates significantly from 1, it may indicate an error in the model or the numerical solution.

CHAPTER 5

Results

5.1. IRRADIATION

After explaining the theoretical background of the problem and introducing the approach behind the simulations, we can now present the results obtained for the model we have developed. The results will always come in pairs, as we have done the same simulations for both the original model, where the frequency factor stays in a constant value (which we will call temperature independent), and the one we propose, where the frequency factor is a function of the temperature following equation 3.16 (temperature dependent). For this first section, we will focus on the graphs obtained from the simulations of the *irradiation* stage of the material. These can be seen in Figures 5.1– 5.3

First and foremost, we can start our analysis of the irradiation stage by looking at the evolution of the occupancy of the traps n_i as a function of time. In Figure 5.1 it is shown that the most prominent difference between the two models lies in what occurs with the trap I, shown by the blue line of n_I . In the temperature independent model, we see that all traps behave in a very similar way; they get gradually filled over time, as the electron-hole pairs are generated. There is a perceptible downward curve in the end of the irradiation time for the n_I trap, which could hint that the trap is being filled to its maximum capacity, but it is not very clear. In the temperature dependent model however, we see that the filling of the n_I trap is much more noticeable, and in turn the growth of the rest of the traps is more pronounced. We see that, without a doubt, the trap I is saturated in the first few minutes of irradiation.

If we look at recombination rates, in Figure 5.2 we can see that both models show a very similar behavior, with the exception of the steep of growth of the radiative recombination rate. In the temperature independent model, the growth is slowed compared to the temperature dependent model, indicating a higher trap occupation. Overall, it is a similar behavior than the one seen in 5.1, as it can be explained with the same principle. When making the frequency factor dependent of temperature, thermal energy dynamics are added, which facilitates the excitation and mobility of our charged carriers. This leads to a higher occupation of traps —beginning with the one closer to the Fermi level, trap I—,

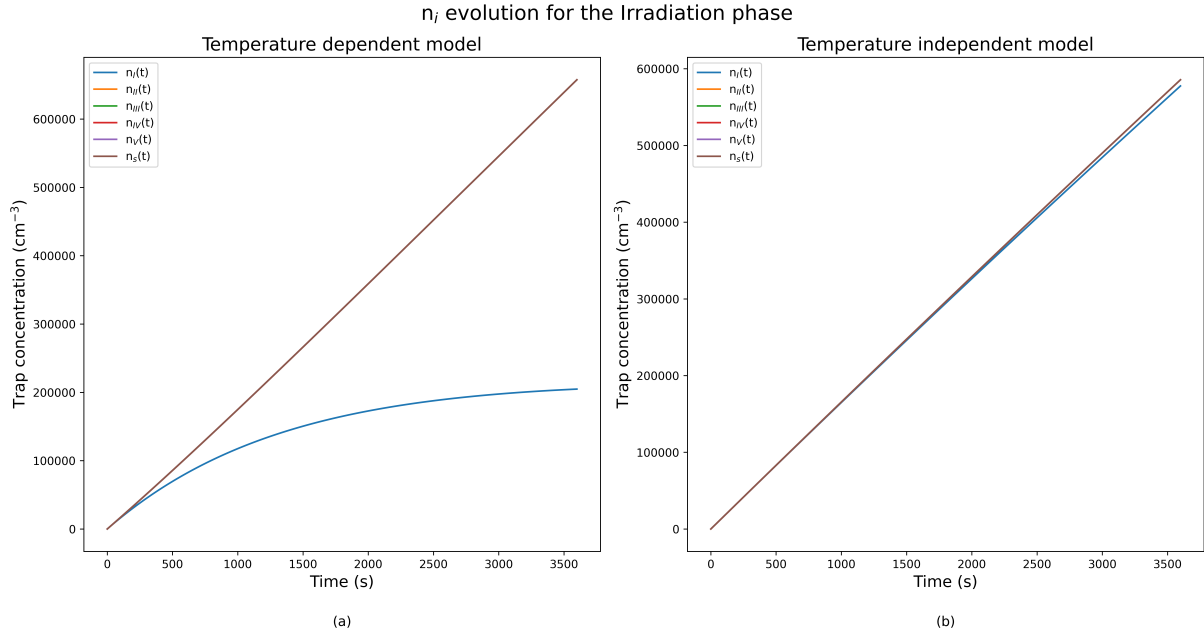


Figure 5.1: Evolution of trap concentrations $n_i(t)$ plotted against time for the $\text{LiF:Mg}, \text{Ti}$ during the irradiation phase for both models (a) Temperature dependent model, where the probabilities of excitation vary with temperature; (b) Temperature independent model, where the excitation probabilities are fixed parameters. Both were subjected to a constant irradiation rate of $G = 1000 \text{ cm}^{-3} \text{ s}^{-1}$ and a laboratory temperature of $T = 25 \text{ }^{\circ}\text{C}$ during 3600 seconds. The traps are labeled as follows: I (blue), II (orange), III (green), IV (red), V (purple), and s (brown).

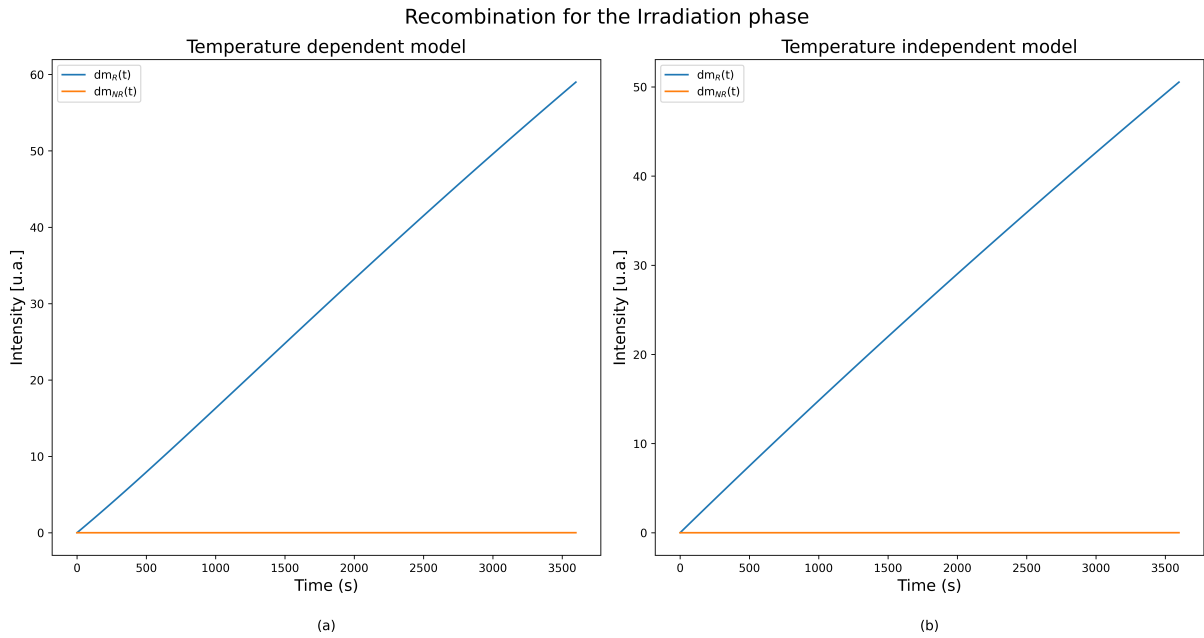


Figure 5.2: Recombination rates during the irradiation phase for both models. (a) Temperature-dependent model; (b) Temperature-independent model. The plotted quantities correspond to the radiative (dm_R/dt) and non-radiative (dm_{NR}/dt) recombination rates. Both models were subjected to a constant irradiation rate of $G = 1000 \text{ cm}^{-3} \text{ s}^{-1}$ and a laboratory temperature of $T = 25 \text{ }^{\circ}\text{C}$ during 3600 seconds.

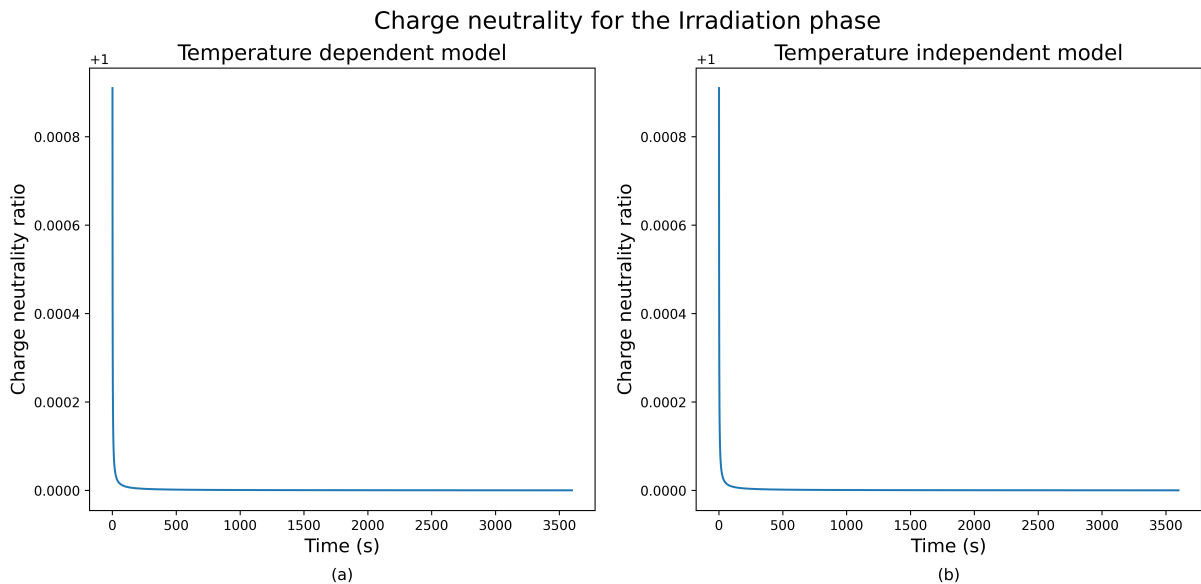


Figure 5.3: Charge neutrality ratio for the LiF:Mg, Ti plotted against temperature during the irradiation phase for both models. (a) Temperature dependent model; (b) Temperature independent model. The plotted ratio corresponds to the total negative charge divided by the total positive charges in the system. Both simulations were performed under a constant generation rate of $G = 1000 \text{ cm}^{-3} \text{ s}^{-1}$ and a laboratory temperature of $T = 25^\circ\text{C}$ during 3600 seconds.

which mathematically translates to higher slope in the graphs. Also, the nearly flat and negligible $dm_{NR}(t)$ in both cases suggests that non-radiative processes play a minimal role under these conditions.

The last graph to analyze is the one introduced in Section 4.2 to validate the model. In Figure 5.3 we can see that both models satisfy the charge neutrality condition, as the total positive and negative charges are approximately equal at all times. The small deviation from the ideal value of 1 is on the order of 10^{-6} , which is negligible and can be attributed to numerical errors in the simulations. This confirms that the model is consistent with the physical principles of charge conservation as introduced in equation 4.1, and that the simulations have been done correctly.

5.2. RELAXATION

After the irradiation stage, we can now analyze the results obtained from the *relaxation* stage of the material. The graphs obtained from the simulations can be seen in Figures 5.4–5.6.

Again, the graphs will be presented in pairs, one for the temperature independent model and one for the temperature dependent model. The first graph to analyze is the evolution of the occupancy of the traps n_i as a function of time, which can be seen in Figure 5.4. At a first glance, one can clearly see a difference between the two figures, divided by one main factor: how does the detrapping work. By keeping the laboratory

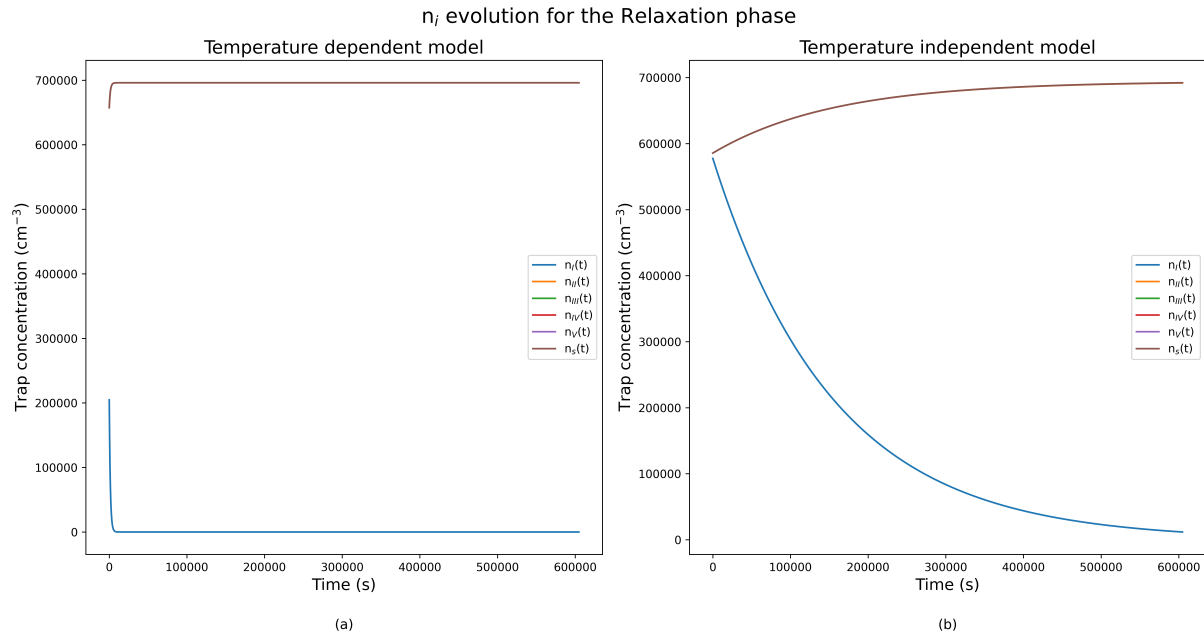


Figure 5.4: Evolution of trap concentrations $n_i(t)$ plotted against time for the LiF:Mg, Ti during the relaxation phase for both models (a) Temperature dependent model; (b) Temperature independent model. Both were subjected to a constant generation rate of $G = 0 \text{ cm}^{-3} \text{ s}^{-1}$ and a laboratory temperature of $T = 25^\circ\text{C}$ during 604,800 seconds. The traps are labeled as follows: I (blue), II (orange), III (green), IV (red), V (purple), and s (brown).

temperature at a fixed value, the probability of thermal detrapping is constant over time, and without electron-hole pair generation, the system evolves solely through the release of previously trapped carriers. As a result, the relaxation dynamics are governed by the intrinsic properties of each trap —specifically the activation energy and frequency factor—, which determine how trapped carriers will evolve.

The decay of the trap I in both models is attributed to the fact that it is the closest trap to the Fermi level, and therefore the one with the lowest activation energy. This means that, even though the frequency factor is constant in the temperature independent model, the carriers will still be able to escape from this trap more easily than from the others. In the temperature dependent model we see that the decay of trap I is much more pronounced, as the thermal dynamics allow for a higher probability of detrapping. The other traps, on the other hand, remain mostly unaffected due to their deeper energy levels, which result in significantly lower detrapping probabilities at the laboratory temperature. This contrast highlights the selective sensitivity of shallow traps to a certain thermal activation temperature, while deeper traps retain their occupancy over longer timescales. It also explains the need for a third stage of the process, where this temperature would be increased to allow the detrapping of all the excited electrons and holes and returning to the equilibrium state from the metastable state the material finds itself in after the relaxation phase.

The next graph to analyze is the one showing the recombination rates during the relaxation stage, which can be seen in Figure 5.5. In this stage, the recombination rate $dm_{R(t)}$ exhibits a sharp decay in both models, consistent with the rapid depletion of free carriers following the irradiation stop. This behavior is driven by the thermal detrap-

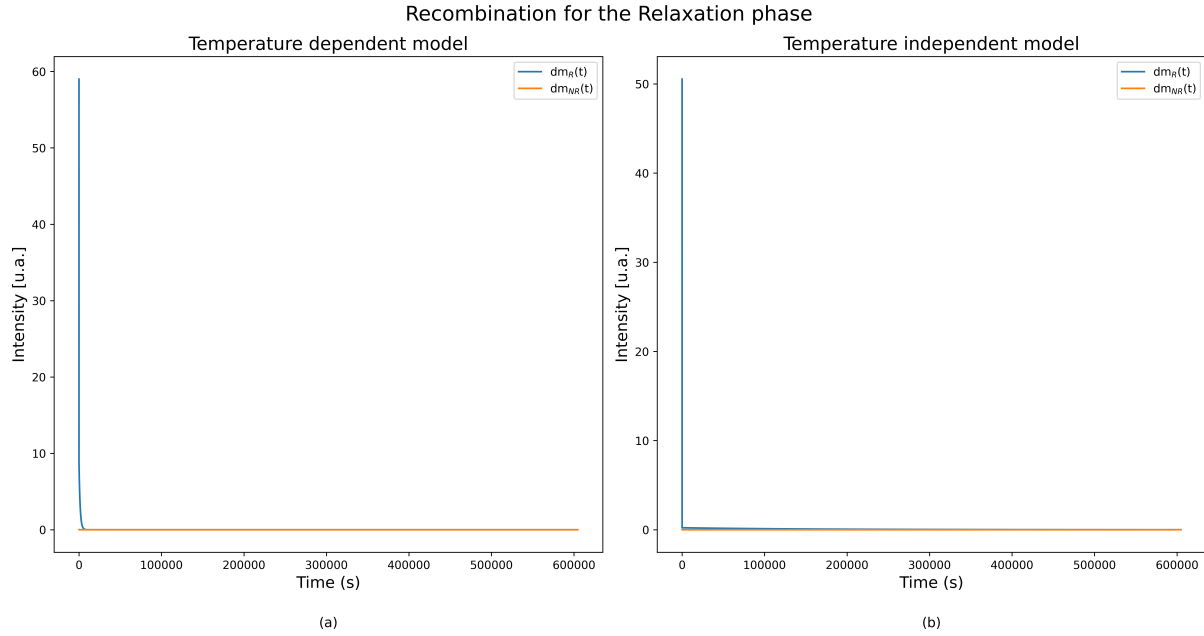


Figure 5.5: Recombination rates for the LiF:Mg, Ti during the relaxation phase for both models. (a) Temperature dependent model; (b) Temperature independent model. The plotted quantities correspond to the radiative (dm_R/dt) and non-radiative (dm_{NR}/dt) recombination rates. Both models were subjected to a constant generation rate of $G = 0 \text{ cm}^{-3} \text{ s}^{-1}$ and a laboratory temperature of $T = 25 \text{ }^\circ\text{C}$ during 604,800 seconds.

ping from the shallow traps —like the trap I we mentioned in the previous paragraph—, which quickly empties when stabilizing the laboratory temperature. Again, the nearly flat $dm_{NR}(t)$ in both cases suggests that non-radiative processes play a minimal role under these conditions.

Although the overall shape of the curves is similar, the temperature dependent model shows a more pronounced decay in the radiative recombination rate. This is due to the fact that, as we have seen in the previous section, the temperature dependent model allows for a higher occupation of traps, which leads to a higher probability of recombination. This is consistent with the fact that the temperature dependent model has a higher slope in the n_i evolution graph, as we saw in Figure 5.1.

The charge neutrality plots shown in Figure 5.6 confirm that the model preserves global charge conservation throughout the relaxation phase. Both the temperature independent and dependent model maintain a nearly perfect balance between positive and negative charges, with only a negligible deviation on the order of 10^{-6} at early times. The stability of these two plots supports the robustness of the simulations done for this phase, and reinforces the consistency of the relaxation dynamics.

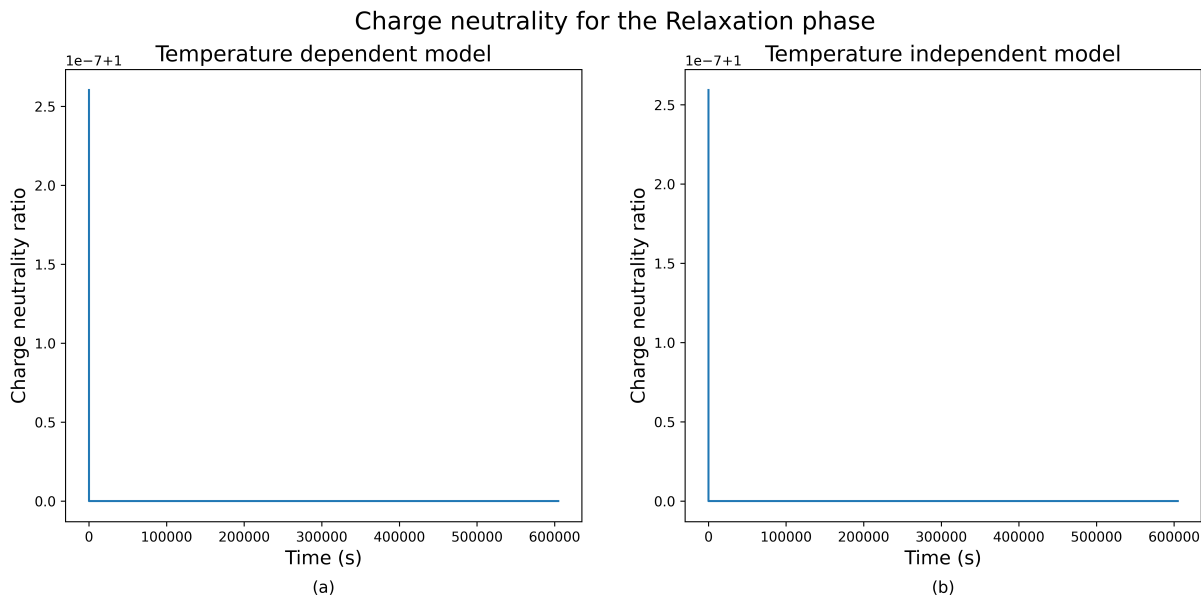


Figure 5.6: Charge neutrality ratio for the LiF:Mg, Ti plotted against temperature during the relaxation phase for both models. (a) Temperature dependent model; (b) Temperature independent model. The plotted ratio corresponds to the total negative charge divided by the total positive charges in the system. Both simulations were performed under a constant generation rate of $G = 0 \text{ cm}^{-3} \text{ s}^{-1}$ and a laboratory temperature of $T = 25^\circ\text{C}$ during 604,800 seconds.

5.3. HEATING

We can now move onto the last stage of the process, the *heating* stage. Here we will obtain the previously introduced TL glow curve, as one of the graphs we have been doing so far. The results obtained from the simulations in this section can be seen in Figures 5.7–5.9.

Before the TL glow curve, we must first analyze what is happening with the occupancy of the traps. Taking now the temperature in our X axis, we can see at a first glance in Figure 5.7, that both models show a similar behavior. As expected, the trap I is the first one to be emptied as it is the closest to the Fermi level. And as it has been seen, it is also here where we see the most significant difference between the two models. The starting point of trap I is notably lower in the temperature dependent model, and can be attributed to thermal detrapping that we have already seen in the irradiation and relaxation stages, all of them due to the influence of the frequency factor. Because trap I we have seen to be shallow, even moderate temperature increase is sufficient to release the charged carriers. In the original model, we see that this trap withstands the temperature a little longer, and is not emptied until surpassing the first 100°C .

The evolution of traps II through V during the heating phase is mostly similar across both models. Each trap empties within its own temperature range, determined by its activation energy. After a certain *activation temperature* T_0 is reached, the traps will experience a sequential release of carriers as temperature increases. On their way to emptying, they will go through a temperature at which the trap releases carriers at the

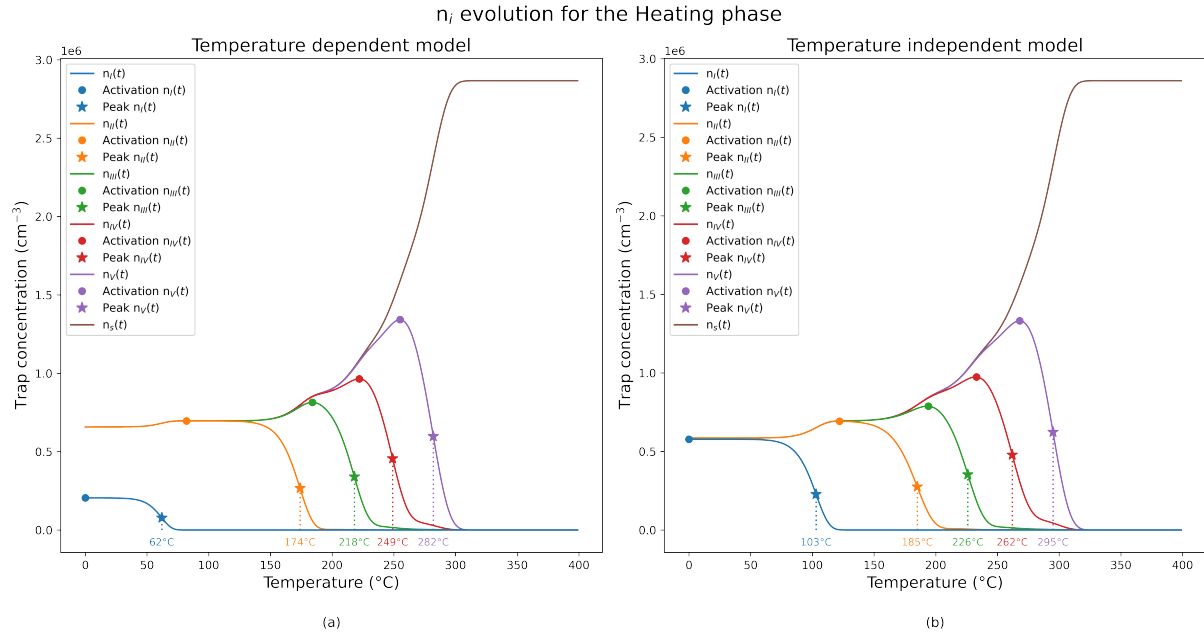


Figure 5.7: Evolution of trap concentrations $n_i(t)$ for the LiF:Mg, Ti plotted against temperature during the heating phase for both models. (a) Temperature dependent model; (b) Temperature independent model. For each trap, both the activation temperature (filled circle) and peak temperature (star icon) are indicated. The peak temperature has a dotted line that reaches the X axis and indicates the specific value for each trap. The simulations were performed under a constant generation rate of $G = 0 \text{ cm}^{-3} \text{ s}^{-1}$ and an increasing laboratory temperature from 0°C to 400°C during 400 seconds. The traps are labeled as follows: I (blue), II (orange), III (green), IV (red), V (purple), and s (brown).

highest rate. This temperature can be called *peak temperature* T_p , and it reflects the characteristic thermal energy required to efficiently empty that trap. It is directly related to the TL glow curve since the luminescence signal is proportional to the rate of carrier release from traps followed by radiative recombination (we remember this from equation 3.8), and therefore each peak observed in the TL glow curve corresponds to this same peak temperature T_p of a trap. Its position and shape provide valuable information about the trap's activation energy, so analyzing the evolution of trap occupancies and identifying their peak temperatures not only characterizes the thermal behavior of the system but also allows the interpretation of the TL glow curve based on the behavior of the traps.

In Figure 5.7, we see that trap s has neither of the characteristic temperatures, as it does not have a maximum. From this we can interpret that it does not follow the same behavior as the other traps because it does not empty at any temperature, but rather accumulates carriers when heated. This is consistent with its energetic position deep in the bandgap closer to the valence band, which implies that an electron captured in this state is highly unlikely, to the temperature range of this experiment, to be thermally re-excited. Such deep levels function as recombination centers rather than trapping states, and represent an irreversible endpoint for charge carriers released from shallower traps during the heating process [1]. For the traps I to V, it is clearly illustrated that the temperature peak depends on the range each trap has for their process of emptying.

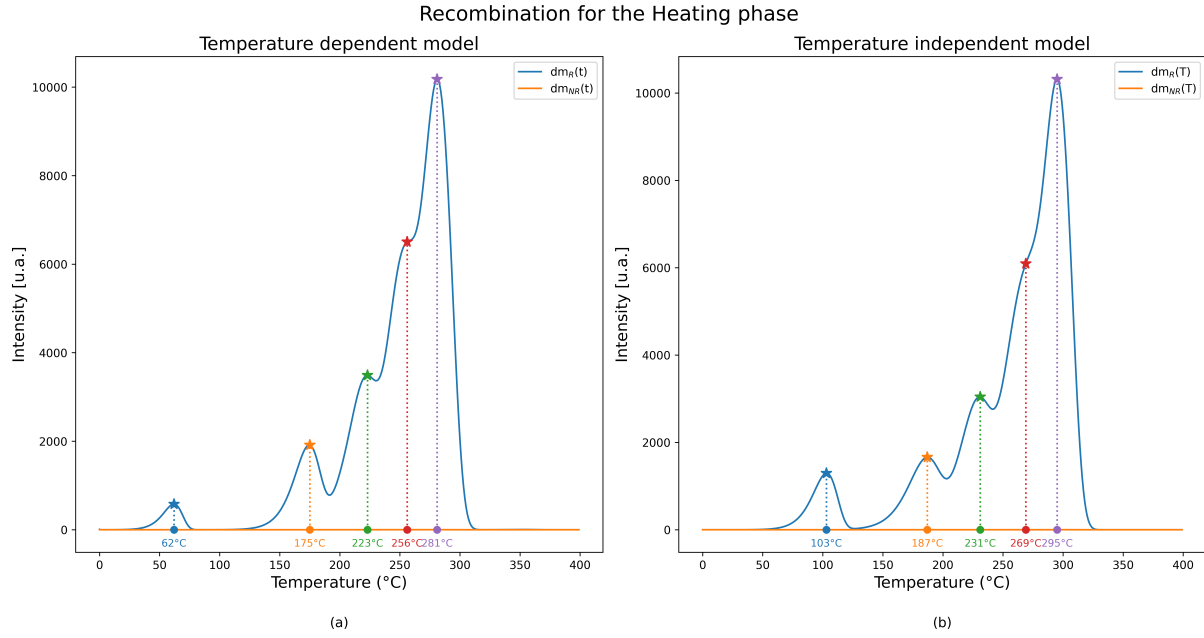


Figure 5.8: Thermoluminescence (TL) glow curves for the $\text{LiF}:Mg, \text{Ti}$ material plotted against temperature during the heating phase for both models. (a) Temperature dependent model; (b) Temperature independent model. The curves correspond to the radiative recombination rate dm_R/dt , showing the intensity of light emitted as trapped carriers recombine. For each visible peak, both the activation temperature (filled circle) and the peak temperature (star icon) are indicated. A vertical dotted line extends from each peak temperature to the X-axis, where the temperature value is labeled. The simulations were performed under a constant generation rate of $G = 0 \text{ cm}^{-3} \text{ s}^{-1}$ and an increasing laboratory temperature from 0°C to 400°C during 400 seconds. The traps are labeled as follows: I (blue), II (orange), III (green), IV (red), V (purple), and s (brown).

And now finally, we can obtain the TL glow curve from the simulations. In Figure 5.8 we can see that both models display the five distinct peaks of $\text{LiF}:Mg, \text{Ti}$, ranging from $\sim 60^\circ\text{C}$ to nearly $\sim 300^\circ\text{C}$, and reflects the increasing activation energies and thermal stability of the traps involved, as the peaks that appear at higher temperatures have higher luminescent response. Comparing both models reveals that the inclusion of temperature dependency in the frequency factor slightly shifts peak positions and modifies peak intensities, particularly in shallower traps. This suggest that the temperature dependency in the frequency factor influences the occupancy dynamics of lower-energy traps.

Furthermore, we can see that indeed the peak temperature values from 5.7 closely match those observed in the TL glow curve for both models. This strong agreement confirms that the temperature at which each trap empties coincides with the point of maximum luminescence intensity in the glow curve. Physically, this reinforces the interpretation that the TL glow peak directly reflects the maximum rate of carrier release from traps. The fact that this correspondence holds in both models despite their fundamental difference suggests that the thermal release of charge carriers is primarily governed by the intrinsic trap properties —such as activation energy, trap activation temperature and frequency factor— rather than by the specific thermal history prior to heating. This implies that the glow peak position is a robust indicator of trap characteristics, such as their activation mechanism, and luminescent response.

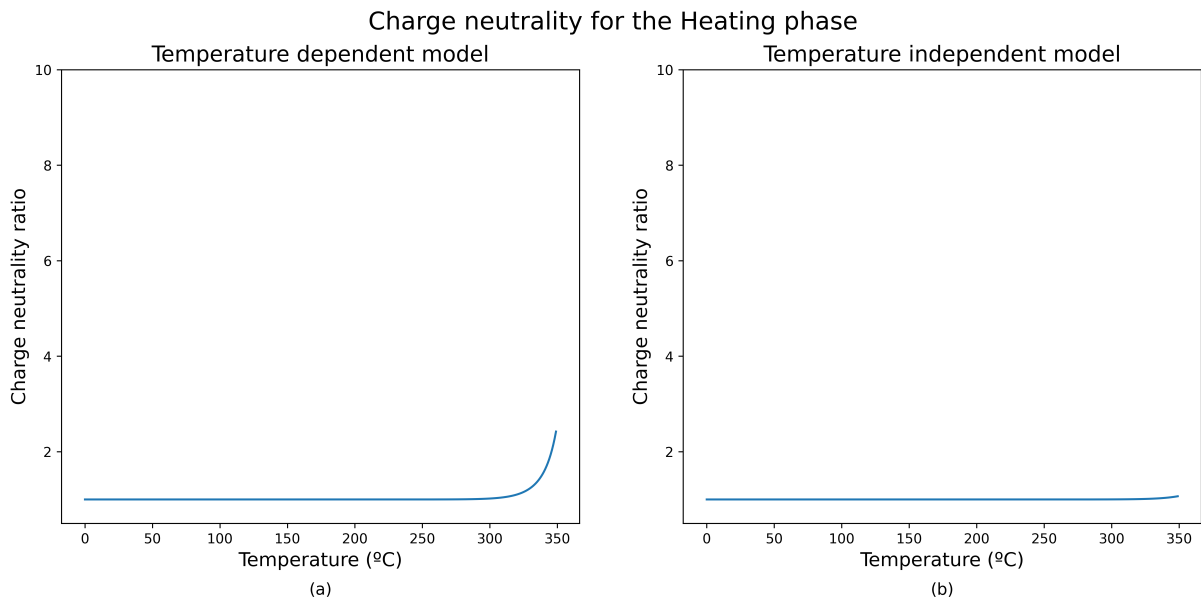


Figure 5.9: Charge neutrality ratio for the $\text{LiF}: \text{Mg}, \text{Ti}$ plotted against temperature during the heating phase for both models. (a) Temperature dependent model; (b) Temperature independent model. The plotted ratio corresponds to the total negative charge divided by the total positive charges in the system. Both simulations were performed under a constant generation rate of $G = 0 \text{ cm}^{-3} \text{ s}^{-1}$ and an increasing laboratory temperature from $0 \text{ }^{\circ}\text{C}$ to $400 \text{ }^{\circ}\text{C}$ during 400 seconds.

As a final note, we can check the validity of the model by looking at the charge neutrality condition, which can be seen in Figure 5.9. As we can see, there is a deviation from the ideal value of 1. A plausible explanation for this is that the temperature increase during the heating phase leads to a higher mobility of the charge carriers. As the temperature increases rapidly during heating, small numerical imbalances between positive and negative charges can become amplified. This is particularly true for the temperature dependent model, where the frequency factor is a function of temperature, leading to a more pronounced effect. Nonetheless, the results still offer a meaningful approximation to the expected physical behavior.

Conclusiones

En este trabajo se ha desarrollado, simulado y analizado un modelo matemático para la respuesta termoluminiscente (TL) del LiF:Mg, Ti, de acuerdo con los objetivos planteados en el Capítulo 2.

Primero, los procesos físicos detrás de la termoluminiscencia se tradujeron en un sistema de ecuaciones diferenciales capaz de describir el comportamiento del material siguiendo una serie de aproximaciones. Desde este punto nacen dos modelos diferentes, que se bifurcan en función de la expresión del factor de frecuencia; un primer modelo, el más simple y usado como referencia, asume un valor constante específico para cada trampa (ecuación 3.15), y un segundo modelo que incorpora una dependencia de la temperatura en el factor de frecuencia basada en la mecánica estadística cuántica (ecuación 3.16).

Ambos modelos han sido implementados en un entorno de simulación numérica que es capaz de solucionar el sistema de ecuaciones diferenciales para las tres fases claves del proceso termoluminiscente: irradiación, relajación y calentamiento. Las simulaciones han conseguido reproducir con éxito el proceso de llenado de las trampas durante la irradiación (Figura 5.1), la consecuente liberación de electrones en la fase de relajación (Figura 5.4), y la liberación térmica final de electrones durante la fase de calentamiento (Figura 5.7). La curva de brillo termoluminiscente obtenida para ambos modelos es consistente con la forma característica del comportamiento experimental del LiF:Mg, Ti (Figura 3.3). Los resultados han sido validados mediante un gráfico de prueba (Figuras 5.3, 5.6 y 5.9) realizado para cada fase, que asegura que el sistema se mantiene eléctricamente neutro.

Tras comparar los resultados de ambos modelos, se ha demostrado que el modelo dependiente de la temperatura es capaz de reproducir mejor el comportamiento de la trampa I, ya que muestra una saturación más rápida durante la irradiación, una disminución más pronunciada en la densidad de electrones durante la relajación y una recombinación más temprana en la fase de calentamiento. También se observa un ligero desplazamiento en la posición e intensidad de los picos en la curva de brillo termoluminiscente (Figura 5.8). Las trampas más profundas, de II a V, exhiben un comportamiento similar en ambos modelos, lo que indica que sus energías de activación, al ser más altas, hacen que sean menos sensibles a la dependencia de temperatura del factor de frecuencia.

Las curvas de brillo termoluminiscente simuladas (Figura 5.8) son bastante similares a los datos experimentales. El gráfico muestra sus cinco picos característicos, cada uno coincidiendo con las temperaturas de activación y pico identificadas en los gráficos de evolución de $n_i(t)$. Esta estrecha correspondencia entre la temperatura de máxima liberación de cada trampa en la Figura 5.7 y su pico luminescente en la Figura 5.8, confirma que los picos de intensidad reflejan de manera fiable las energías de activación de las trampas y sus probabilidades de recombinación.

En resumen, este estudio no solo reproduce el comportamiento termoluminiscente visto experimentalmente en el LiF:Mg, Ti mediante simulación por ordenador, sino que también demuestra que la introducción de una dependencia de la temperatura en el factor de frecuencia puede mejorar la capacidad del modelo para explicar la dinámica de los portadores de carga involucrados en el proceso. Estos hallazgos subrayan la importancia del sutil efecto de la temperatura en el modelado termoluminiscente, y abren camino para futuros trabajos que refinen aún más el modelo, potencialmente incorporando una dependencia de temperatura más compleja. El contenido de este Trabajo Fin de Grado se presentará en la 51^a Reunión Anual de la Sociedad Nuclear Española el 24 de septiembre de 2025.

Conclusions

In this work, a mathematical model for the thermoluminescent (TL) response of LiF:Mg, Ti was developed, simulated and analyzed in accordance with the objectives set out in Chapter 2.

First, the underlying physical processes of thermoluminescence were translated into a set of differential equations capable of describing the behavior of the material with a series of approximations. Two different models branched out over the temperature dependency in the electron's frequency factor (equation 3.15); the first and most simple one assumed a constant value and was used as a reference, and the second one incorporated a temperature dependency based on quantum statistical mechanics (equation 3.16).

Both models were then implemented in a numerical simulation environment that was able to solve these equations across all three key phases of the TL process: irradiation, relaxation and heating. The simulations successfully reproduced the processes of filling of traps during irradiation (Figure 5.1), the subsequent liberation of electrons in the relaxation phase (Figure 5.4), and the final thermal release of electrons during the heating phase (Figure 5.7). The TL glow curves obtained for both models were consistent with the characteristic shape of the experimental behavior of LiF:Mg, Ti (Figure 3.3). The results were validated through a test graph (Figures 5.3, 5.6, and 5.9) done for every phase, that assured that the system stayed electrically neutral.

A comparison between the two models was made, and revealed that the temperature dependent model was able to better reproduce the behavior of trap I, showing earlier saturation during irradiation, a steeper decrease in occupancy during relaxation and an early recombination in the heating phase. It also showed a slight shift in peak position and intensity in the glow curve (Figure 5.8). In contrast, deeper traps from II to V exhibited similar behavior in both models, indicating that their higher activation energies rendered them less sensitive to the frequency factor's temperature dependency.

The simulated TL glow curves (Figure 5.8) display a good agreement with the experimental data. The plot displays its five distinct peaks, each matching the activation and peak temperatures identified from the $n_i(t)$ evolution plots. The close correspondence between each trap's maximum release rate temperature (Figure 5.7) and its luminescent peak (Figure 5.8) confirms that the glow peaks reliably reflect the trap activation energies and recombination probabilities.

In summary, this study not only reproduces the known TL behavior of LiF:Mg, Ti via computer simulation, but also demonstrates how introducing a temperature dependency in the frequency factor can enhance the model's ability to explain the dynamics of the charge carriers involved in the process. These findings underscore the importance of the

subtle effect of temperature in the TL modeling, and pave way for future work to refine the model further, potentially incorporating a more complex temperature dependency. The contents of this final thesis will be presented in the 51st Annual Meeting of the Spanish Nuclear Society on the 24th of September 2025.

Bibliography

- [1] McKeever, Stephen W. S. (2022). *A course in luminescence measurements and analyses for radiation dosimetry*. Wiley. ISBN 978-1-119-64689-1.
- [2] F. J. F. Arenas, "Study on photo-ionization cross-sections through the simulation of the behaviour of crystalline materials used in dosimetry," unpublished undergraduate thesis.
- [3] J. J. Brey Abalo, *Mecánica estadística*, 1a ed., 6a reimp. Madrid: Universidad Nacional de Educación a Distancia, 2020. Colaboradores: J. de la Rubia Pacheco y J. de la Rubia Sánchez. ISBN: 978-84-362-4572-1.
- [4] J. F. Benavente, J. M. Gómez-Ros, and A. M. Romero, "Numerical analysis of the irradiation and heating processes of thermoluminescent materials," *Radiation Physics and Chemistry*, vol. 170, p. 108671, May 2020. doi: 10.1016/j.radphyschem.2019.108671.
- [5] Y. S. Horowitz, L. Oster, and H. Datz, The thermoluminescence dose response and other characteristics of the high-temperature TL in LiF:Mg,Ti (TLD-100), *Radiation Protection Dosimetry*, vol. 124, no. 2, pp. 191–205, Jun. 2007, doi: 10.1093/rpd/ncm241.
- [6] G. Massillon-JL, C. S. N. Johnston, and J. Kohanoff, "On the role of magnesium in LiF:Mg,Ti thermoluminescent dosimeter," *Journal of Physics: Condensed Matter*, vol. 30, no. 12, p. 125701, 2018. doi: 10.1088/1361-648X/aaee62.
- [7] B. H. Bransden and C. J. Joachain, *Physics of Atoms and Molecules*, 2nd ed. Harlow, England: Pearson Education, 2003.
- [8] Y. S. Horowitz, L. Oster, and H. Datz, "The thermoluminescence dose response and other characteristics of the high-temperature TL in LiF:Mg,Ti (TLD-100)," *Radiation Protection Dosimetry*, vol. 124, no. 2, pp. 191–205, Jun. 2007. doi: 10.1093/rpd/ncm241.
- [9] Halimi Mokhtar, Dahane Kadri, and Abdelmalek Mokeddem, "Simulation of the experimental thermal cleaning procedure in LiF:Mg,Ti and investigation of the origin of the first-order kinetics of its peaks," *Modern Physics Letters B*, vol. 29, no. 35, p. 1550226, Dec. 2015, doi:10.1142/S0217984915502267.
- [10] S. W. S. McKeever, *Thermoluminescence of Solids*. Cambridge University Press, 1985. doi: 10.1017/CBO9780511564991.